$\text{LiMg}_{y1}\text{Cr}_{y2}\text{Mn}_{2-y1-y2}\text{O}_4$ ($0.0 \leq y_1 \leq 0.30$; $y_2 = 0.30 - y_1$) as a Cathode Active Material for Lithium Batteries

N. Kalaiselvi,[*] R. Thirunakaran, P. Periasamy, M. Sakthivel, N. Muniyandi

Lithium Batteries Section, Advanced Batteries Division, Central Electrochemical Research Institute, Karaikudi-630 006, Tamil Nadu, India

Abstract

LiMn_2O_4 is an attractive 4 V positive material in lithium rechargeable batteries owing to its favourable electrochemical characteristics besides its economic and environmental advantages. However, problems of limited cyclability, especially at elevated temperatures, have limited the utility and commercialization of this cathode material. Stabilization of the LiMn_2O_4 spinel structure has been sought to be realized by doping the spinel with suitable cations. In this paper, the results of an exploratory research on the capacity and cyclability of LiMn_2O_4 cathodes simultaneously doped with Cr^{3+} and Mg^{2+} are reported. $\text{LiMg}_{y1}\text{Cr}_{y2}\text{Mn}_{2-y1-y2}\text{O}_4$ spinels with $y_1 = 0.00$, 0.05, 0.10, 0.20, 0.25 and 0.30 and y_2 ($0.3 - y_1$) were synthesized by a solid-state fusion method. While Mg^{2+} bestows a positive effect on cyclability, it leads to a considerable reduction in capacity due to the oxidation of Mn^{3+} to the inactive Mn^{4+} as a result of charge compensation. Cr^{3+} on the other hand, leads only to half as much reduction in capacity while according added stability to the structure. Any expectation of a synergistic effect by Cr^{3+} and Mg^{2+} ions was belied by these findings.

Keywords: magnesium, chromium, LiMn_2O_4, cyclic voltammetry, impedance measurements, lithium battery cathode.

Introduction

The LiMn_2O_4 spinel with a theoretical charge density of 148 mAh/g, flat discharge profile, low cost and non-toxicity, is a promising cathode active material for rechargeable lithium batteries. It cycles well at room temperature, although prolonged cycling at high temperatures is accompanied by a capacity fade [1,2]. The capacity fade has been attributed to manganese dissolution [3],

---

[*] Corresponding author. E-mail address: cecrik@cscecri.ren.nic.in

Jahn-Teller distortion [4] and lattice instability [5]. Several approaches, including doping of the spinel with transition and non-transition metal ions, have been adopted to enhance the cyclability of the spinel [6-17]. For example, doping with cobalt, nickel or chromium imparted increased cyclability at the expense of capacity [10-12]. Of late, Sigala *et al.* [18] demonstrated the beneficial role of substitution towards $LiMn_2O_4$ cyclability. The substitution of other elements such as Al, V, Ga, and Zn for Mn could also lead to increased stability of the spinel structure as manifested in the increased cycling performance of the doped compounds [6,9,14-17]. In the work presented here, we have made an attempt to stabilize the spinel structure by simultaneously doping with trivalent chromium and divalent magnesium. The stoichiometries of magnesium (y_1) employed were 0.00, 0.05, 0.10, 0.20, 0.25 and 0.30 and those of chromium (y_2) were such that $y_2 = 0.3 - y_1$.

Experimental

Preparation of $LiMg_{y1}Cr_{y2}Mn_{2-y1-y2}O_4$ cathode material

$LiMg_{y1}Cr_{y2}Mn_{2-y1-y2}O_4$ powders were prepared by a solid-state fusion method. Stoichiometric amounts of carbonates of lithium, magnesium and manganese, and ammonium dichromate were thoroughly mixed in n-hexane for about 12 h. The solvent was subsequently evaporated and the solid mass was heat treated initially at 673 K for 6 h and then at 1073 K for 72 h with intermittent grinding. The fine powders obtained were collected and subjected to various physical and electrochemical characterization studies.

Instruments

Powder X-ray diffraction patterns were recorded on a Jeol JDX 8030 X-ray difractometer with a nickel-filtered Cu-Kα radiation. FTIR spectra were recorded on a Perkin-Elmer FTIR spectrophotometer using the KBr pellet method. For thermal analytical studies an STA 1500 simultaneous thermal analysis system of polymer laboratories was employed. AC impedance measurements were carried

out using a Princeton Applied Research Potentiostat / Galvanostat (EG & G Instruments, Model 6310, USA).

Electrode preparation

The synthesized powders were mixed with 10 % acetylene black in N-methyl-2-pyrrolidone containing 5 % poly(vinylidene fluoride) to form a slurry. The slurry was then coated on an aluminum foil substrate and dried in an oven at 393 K for 24 h. Discs of 18 mm diameter were punched out from these foils; active material loaded on the substrate was 0.082 – 0.096 g. Coin cells of 2016 configuration were assembled in an M Braun glove box with lithium foil as the anode, 1 M LiAsF$_6$ in a 30:70 (v/v) mixture of dimethyl carbonate and the ethylene carbonate as the electrolyte and Celgard 2400 as the separator. All charge-discharge studies were carried out using in-house assembled battery testing unity.

Results and discussion

Thermal analysis

TG/DTA curves obtained with the precursors for LiMg$_{y1}$Cr$_{y2}$Mn$_{2-(y1+y2)}$O$_4$ with y$_1$ = 0.30, 0.25, 0.20, 0.10, 0.00 and y$_2$ = 0.00, 0.05, 0.10, 0.20 are shown in Fig. 1a-1e, respectively.

All the profiles show a low temperature region up to about 600 K followed by a high temperature region. The low temperature region may be attributed to any dehydration and to the decomposition of MnCO$_3$ to MnO and CO$_2$ which is expected to begin at 473 K [19]. (NH$_4$)$_2$Cr$_2$O$_7$, if present in the precursor, may also be expected to give a decomposition profile in this temperature region. The decomposition of the latter to N$_2$, H$_2$O and Cr$_2$O$_3$ occurs at 438 K.
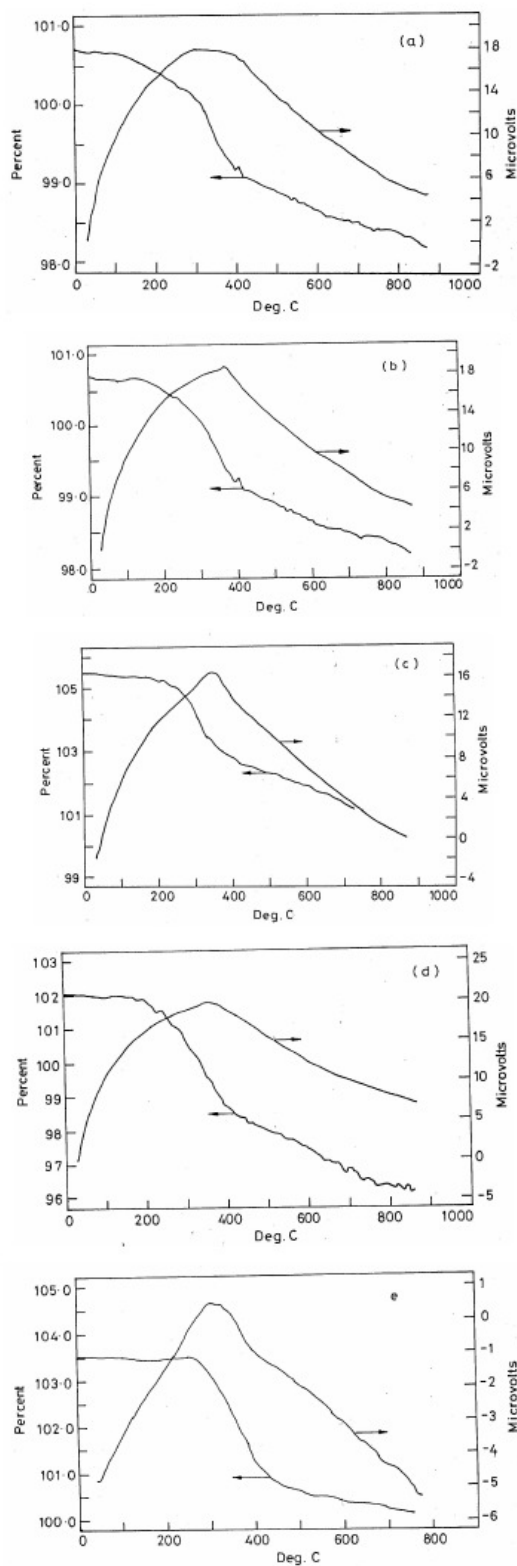
Figure 1. TG/DTA curves of $LiMg_{y1}Cr_{y2}Mn_{2-(y1+y2)}O_4$ samples (a-e). a) $y_1 = 0.00$, $y_2 = 0.00$; b) $y_1 = 0.10$, $y_2 = 0.20$; c) $y_1 = 0.20$, $y_2 = 0.10$; d) $y_1 = 0.25$, $y_2 = 0.05$; e) $y_1 = 0.30$, $y_2 = 0.00$.

Although no discernible difference could be observed in the TG profiles (Fig. 1a-1d), they do differ from that of Fig. 1e: in that the former slope down slowly while the TG in Fig. 1e has a sharp slope in the 450 – 700 K region that is clearly attributable to the absence of $MgCO_3$ in Fig. 1e. The decomposition of anhydrous $MgCO_3$ begins at around 673 K and grains rapidly above 820 K [20]. Although Li_2CO_3 is stable in air up to 1023 K with a melting point of 998 K [21], the extended exothermic region may be attributed to a possible reaction between the finely divided $MnO/Cr_2O_3/MgO$ and Li_2CO_3 to form Mn-Cr-Mg oxide with interstitial Li_2O as has been observed with the case of $CoCO_3$ and Li_2CO_3 mixtures [22]. The results are not unexpected given the fact that several carbonates upon mixing produce easily decomposable mixtures [23]. Carbon dioxide, a product of the decomposition reaction, in the reaction zone is believed to trigger the melting of an eutectic of composition Li_2CO_3-Li_2O-LiOH around 683 K [24,25]. The high temperature region is leading to the formation of the final products.

Structural considerations

Fig. 2 shows the X-ray diffraction patterns of $LiMn_2O_4$ and $LiMg_{y1}Cr_{y2}Mn_{2-(y1+y2)}O_4$ with various concentrations of y_1 and y_2 powders (Fig. 2a-2f). The similarity of the diffraction pattern suggests that the original spinel structure (symmetry: Fd3m) was maintained at all dopant concentrations, and that no impurity phases were formed. Maintenance of the spinel structure when a part of Mn at the 16d site in $LiMn_2O_4$ is substituted with Mg or Cr has been studied by many researchers [10,26,27].

Similarly, closeness of lattice parameters values of the doped $LiMn_2O_4$ as compared to the undoped one has also been noted [28-31]. The average oxidation state of Mn ions gradually increases with the increasing of Mg content which should result in a shrinkage of the unit cell volume. This is also because of the fact that at the same oxidation state, chromium ions have smaller ionic radii than manganese ions: Cr^{3+} (0.0615 Å), Mn^{3+} (0.68 Å), Cr^{4+} (0.58 Å), Mn^{4+} (0.60 Å) [32]. Ionic radii of both Cr^{3+} and Mg^{2+} are smaller than that of Mn^{3+} and,

therefore, doping with trivalent chromium and magnesium results in the shift of peaks towards higher angles. The increased average oxidation state of manganese means proportional reduction in the amount of Jahn-Teller Mn^{3+} ions which must manifest in increased stability of the Mg doped $LiMn_2O_4$. The structural stability of the doped $LiMn_2O_4$ is also increased because of the high stabilization energy for octahedral co-ordination Cr^{3+} ions [33]. Indeed, the incorporation of Cr^{3+} greatly suppresses the dissolution of manganese ions in the electrolyte (one of the failure mechanisms of the $LiMn_2O_4$ cathode) [18] via the following disproportionation reaction:
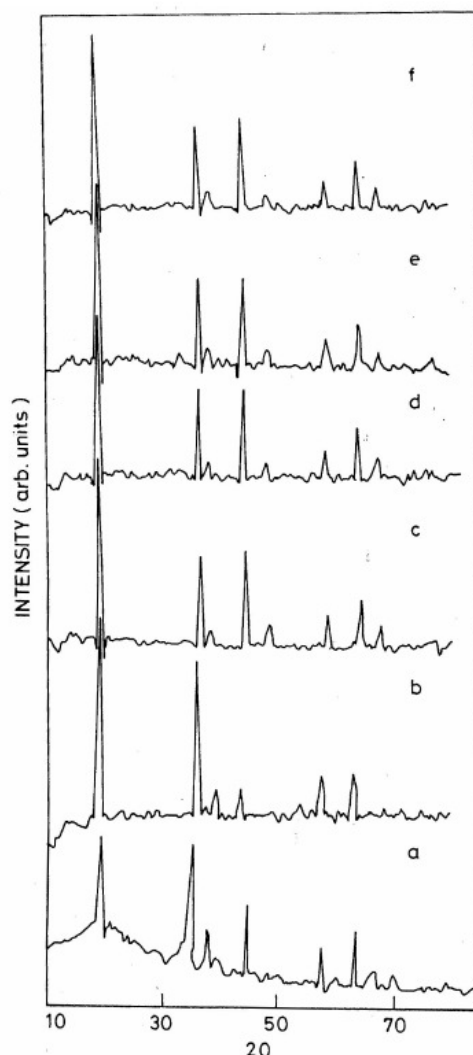
$$2 \, Mn^{3+} \rightarrow Mn^{4+} + Mn^{2+}$$

Figure 2. Powder XRD patterns of $LiMg_{y1}Cr_{y2}Mn_{2-(y1+y2)}O_4$ samples (a-f). a) $y_1 = 0.00$, $y_2 = 0.00$; b) $y_1 = 0.10$, $y_2 = 0.20$; c) $y_1 = 0.20$, $y_2 = 0.10$; d) $y_1 = 0.25$, $y_2 = 0.05$; e) $y_1 = 0.30$, $y_2 = 0.00$; f) $y_1 = 0.35$, $y_2 = 0.00$.

FTIR spectrum of $LiMn_2O_4$ (Fig. 3) consists of two featureless bands around 530 cm^{-1} and 620 cm^{-1}. The large difference in mass, volume and charge of lithium as compared to the transition metals may mean that one or more peaks associated with the movement of lithium ions may be dominating the rest.
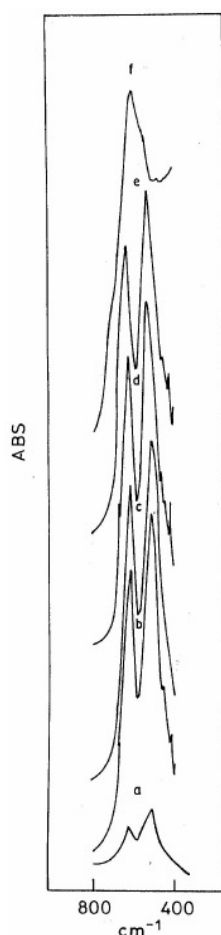

Figure 3. FTIR spectra recorded for $LiMg_{y1}Cr_{y2}Mn_{2-(y1+y2)}O_4$ samples (a-f). a) $y_1 = 0.00$, $y_2 = 0.00$; b) $y_1 = 0.10$, $y_2 = 0.20$; c) $y_1 = 0.20$, $y_2 = 0.10$; d) $y_1 = 0.25$, $y_2 = 0.05$; e) $y_1 = 0.30$, $y_2 = 0.00$; f) $y_1 = 0.35$, $y_2 = 0.00$.

According to Richardson et al. [34] the peak around 620 cm^{-1} is due to $[LiO_4]$ tetrahedral units while the one around 530 cm^{-1} is due to the octahedral to tetragonally distorted unit of $[MnO_6]$ units. However, the dopants which occupy octahedral sites shift the $[MnO_6]$ peak to slightly higher wave numbers (around 540-550 cm^{-1}). FTIR spectra thus indirectly suggest the presence of a solid

mixing or due to a second phase may thus be ruled out. A less pronounced peak at 560 cm^{-1} for $y_1 = 0.3$ may be due to the fact that increased amounts of Mg in the solid solution may induce some cation distribution [35].

Electrochemical features

The cells were discharged at 0.1 mA rate between a potential range of 3.2-4.9 V. Fig. 4 shows the first discharge curves of $LiMg_{y1}Cr_{y2}Mn_{2-(y1+y2)}O_4$. Electrochemical insertion of lithium from $LiMg_{y1}Cr_{y2}Mn_{2-(y1+y2)}O_4$ spinels occurs in two steps.
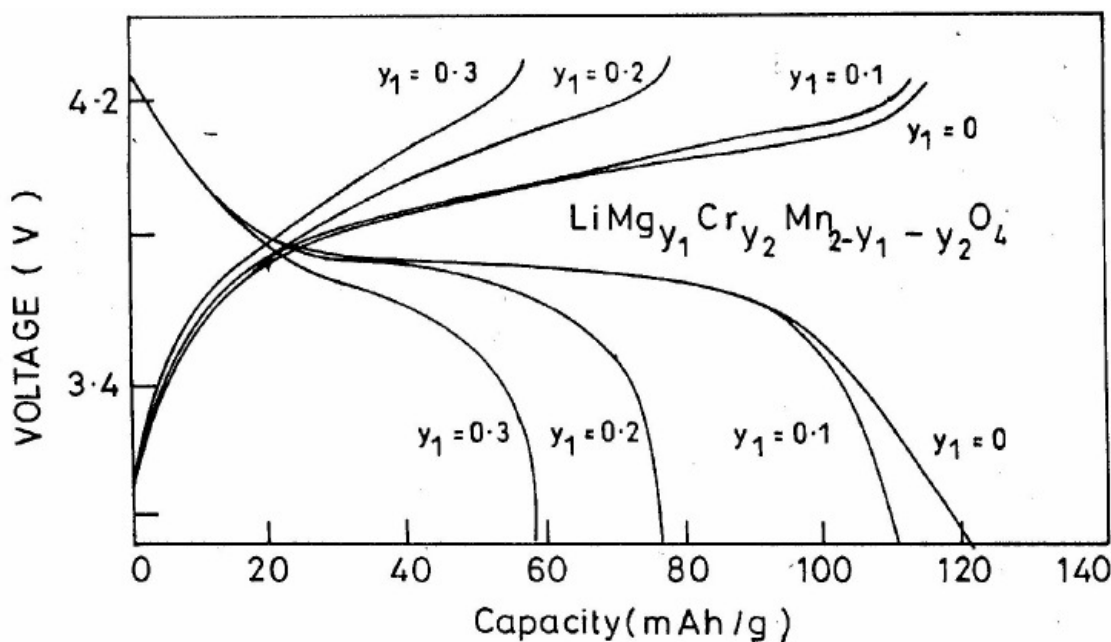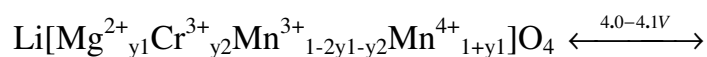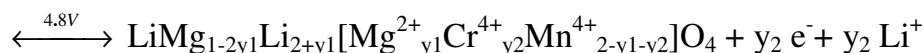

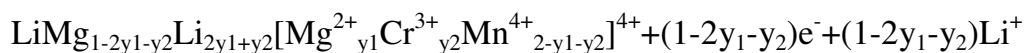**Figure 4.** Charge-discharged curves of $Li/LiMg_{y1}Cr_{y2}Mn_{2-(y1+y2)}O_4$ with various concentrations of Mg doped cells. Drain rate: 0.1 mA.

The first voltage at around 4.0 V corresponds to the oxidation of Mn^{3+} to Mn^{4+} while the second one at around 4.8 V corresponds to the oxidation of Cr^{3+} to Cr^{4+} [11,12]. The two step lithium intercalation/deintercalation reaction may be represented as follows:

$$Li[Mg^{2+}_{y1}Cr^{3+}_{y2}Mn^{3+}_{1-2y1-y2}Mn^{4+}_{1+y1}]O_4 \xleftrightarrow{\ 4.0-4.1V\ }$$

$$LiMg_{1-2y1-y2}Li_{2y1+y2}[Mg^{2+}_{y1}Cr^{3+}_{y2}Mn^{4+}_{2-y1-y2}]^{4+}+(1-2y_1-y_2)e^-+(1-2y_1-y_2)Li^+$$

$$\xrightarrow{\text{4.8V}} LiMg_{1-2y1}Li_{2+y1}[Mg^{2+}_{y1}Cr^{4+}_{y2}Mn^{4+}_{2-y1-y2}]O_4 + y_2\ e^- + y_2\ Li^+$$

Thus we see that an amount equal to $2y_1$ (twice the stoichiometry of the divalent magnesium) is theoretically unavailable for electrochemical cycling. The theoretical capacities at the 4 V region and the average manganese oxidation states for the various compositions are tabulated in Table 1.

Table 1. Theoretical and observed capacities in the 4 V region for $LiMn_2O_4$ doped with Cr^{3+} and Mg^{2+}.

Compound	Specific Capacity / (mAh/g)		Average Mn oxidation state
	Observed	Theoretical	
$LiMn_2O_4$	128.0	148.0	3.50
$LiMg_{0.05}Cr_{0.25}Mn_{1.7}O_4$	86.0	96.2	3.62
$LiMg_{0.10}Cr_{0.20}Mn_{1.7}O_4$	80.1	90.8	3.65
$LiMg_{0.20}Cr_{0.10}Mn_{1.7}O_4$	68.5	76.9	3.71
$LiMg_{0.25}Cr_{0.05}Mn_{1.7}O_4$	62.7	69.7	3.74
$LiMg_{0.3}Mn_{1.7}O_4$	57.5	62.5	3.76

Among the doped compounds, $LiMg_{0.10}Cr_{0.20}Mn_{1.7}O_4$ has improved cycling performance indicating the best stabilized composition studied. The increased stability of this compound as manifested in increased cyclability (reduced capacity fade) may be attributed to the smaller radii of Mg^{2+} [6,23] and Cr^{3+} as compared to Mn^{3+} as well as to the preference of Cr^{3+} ions for octahedral sites. Fig. 5 shows the discharge capacities of $LiMg_{y1}Cr_{y2}Mn_{2-(y1+y2)}O_4$ and $LiMn_2O_4$ upon cycling up to 20 cycles. From Fig. 5, it is seen that the capacity fade per cycle for $LiMn_2O_4$ is large as compared to that for $LiMg_{0.10}Cr_{0.20}Mn_{1.7}O_4$. $LiMn_2O_4$ with Mg and Cr leads to improved cycling performance due to improved stabilization of the structure.

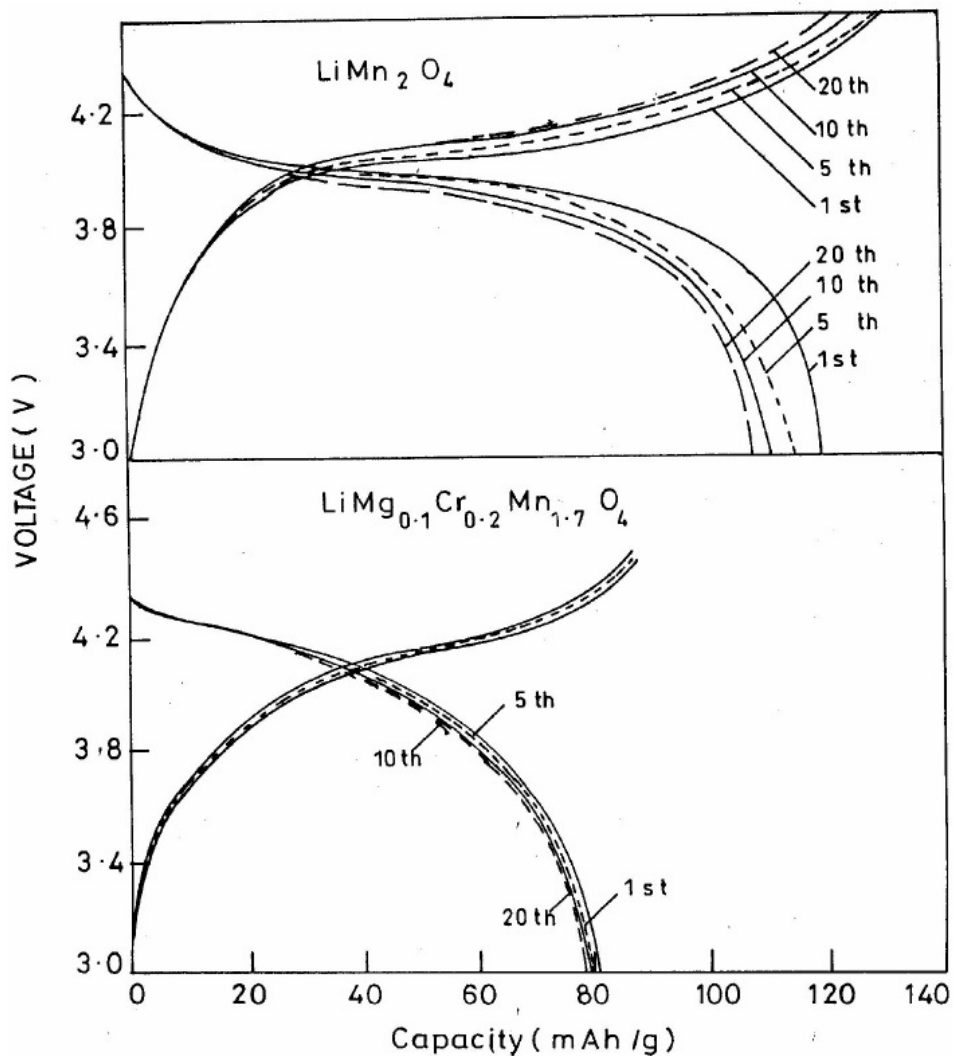**Figure 5.** Charge-discharged curves of Li/LiMn$_2$O$_4$ and Li/LiMg$_{0.1}$Cr$_{0.2}$Mn$_{1.7}$O$_4$ cells. Drain rate: 0.1 mA.

Cyclic voltammograms (sweep rate: 1 mV/sec) of the cells employing LiMn$_2$O$_4$ and LiMg$_{0.10}$Cr$_{0.20}$Mn$_{1.7}$O$_4$ are presented in Fig. 6. At small concentrations, the dopants lead to a decrease in the anodic/cathodic peak separation indicating an improvement in the electrochemical reversibility of the doped cathode material.
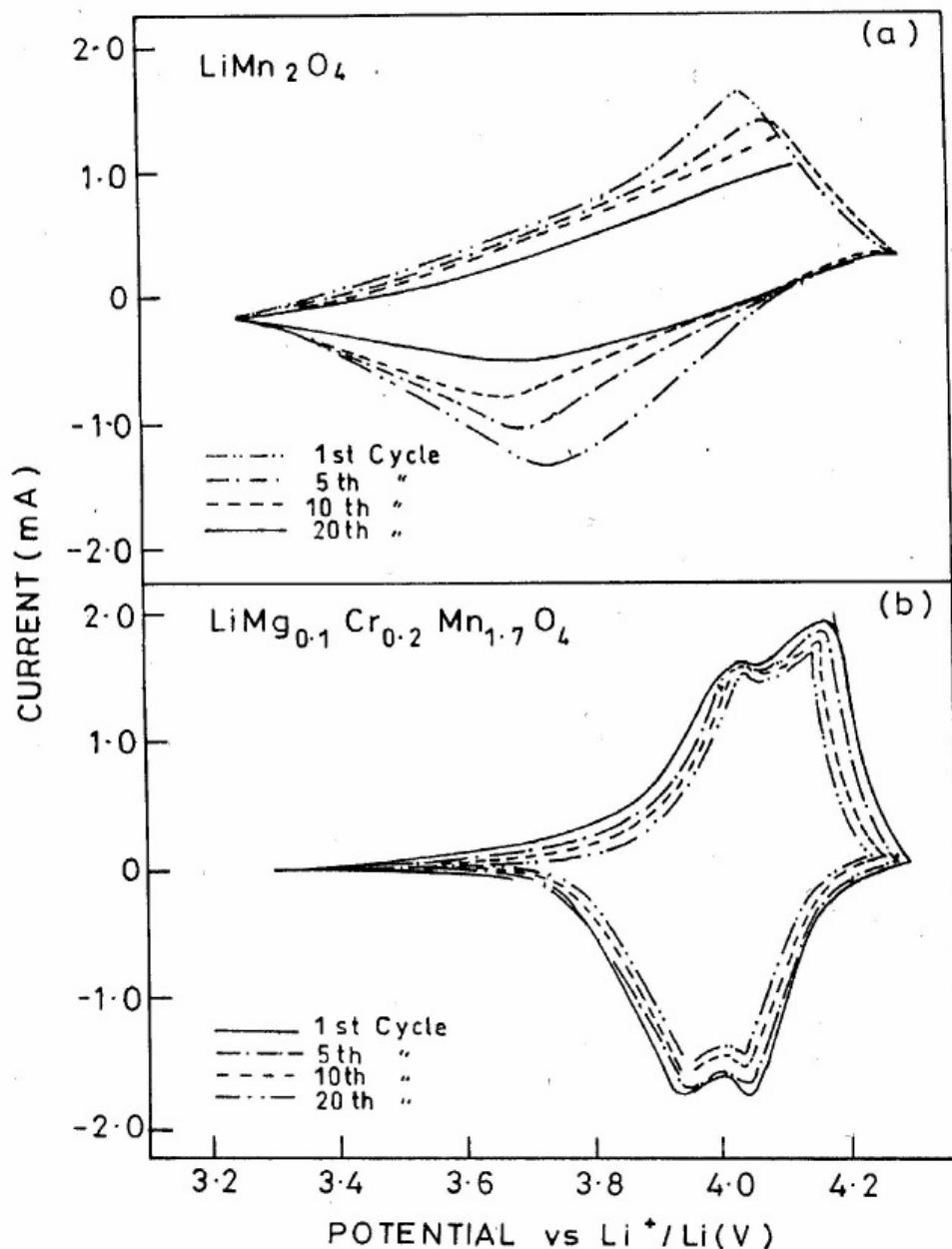
Figure 6. Cyclic voltammograms of cells containing: (a) $LiMn_2O_4$ and (b) $LiMg_{0.1}Cr_{0.2}Mn_{1.7}O_4$ (1st, 5th, 10th and 20th cycles). Sweep rate: 1 mV/sec.

Fig. 6 shows the cyclic voltammograms at the 1st and 20th cycles for pure $LiMn_2O_4$ and $LiMg_{y1}Cr_{y2}Mn_{2-(y1+y2)}O_4$. The improved reversibility of the doped compound is reflected in the closeness of the cyclic voltammograms obtained at the first and twentieth cycles. Further, there is definite increase in the peak currents as the cycling proceeds for the doped samples containing to what is observed for $LiMn_2O_4$. This too suggests improved cyclability of the doped $LiMn_2O_4$. Two anodic peaks in anodic direction and two cathodic peaks in cathodic direction were observed for $LiMn_2O_4$ when compared to the initial

values. The observed shift of the peak potential in the case of $LiMn_2O_4$ is indicative of the increased instability upon cycling. This shift is found to be reduced in the cyclic voltammograms of the doped spinel, $LiMg_{y1}Cr_{y2}Mn_{2-(y1+y2)}O_4$, apart from the stabilization imparted to the structures through reduced unit cell volumes by Mg^{2+} and Cr^{3+} and octahedral site stabilization by Cr^{3+}, and additional feature in the Mg^{2+} containing spinels in the increased average oxidation state of Mn. Thus, the reduction in the amount of Jahn-Teller ion, Mn^{3+} also contributes to structure stabilization.

Coin cells with $LiMn_2O_4$ and $LiMg_{0.10}Cr_{0.20}Mn_{1.7}O_4$ were subjected to electrochemical impedance measurements. The frequency range covered was 0.01 Hz to 100 Hz at a 5 mV signal. All cells were tested in their discharged states (cut-off voltage: 3.2 V). Nyquist plots were recorded at the end of the 1st, 5th, 10th and 20th cycles (Fig. 7). It may be seen from the figure that although the charge transfer resistance of the two cells was similar at the end of the first cycle, the difference between them steadily increased. The values for the cells with doped cathode material was always higher indicating a slower rate of passivation of the electrode surface.

Conclusions

$LiMg_{y1}Cr_{y2}Mn_{2-(y1+y2)}O_4$ solid solutions have been synthesized using a solid-state fusion method. Cr substituted compounds show a voltage plateau at approx. 4.8 V corresponding to the Cr^{4+}/Cr^{3+} couple and one around 4.0 V corresponding to the Mn^{4+}/Mn^{3+} couple. Although the Cr and Mg substituted compounds show reduced discharge capacities their cycling capabilities are higher compared to the pristine $LiMn_2O_4$. The higher octahedral stabilization energy of Cr^{3+} and the contraction of unit cell volume upon incorporation of Cr^{3+} and Mg^{2+} contribute to greater structural stability to doped spinels as may be deduced from reduced capacity fade upon cycling. Among the compositions studied $LiMg_{0.05}Cr_{0.25}Mn_{1.7}O_4$ qualifies as a potential cathode material with long cycling capability.

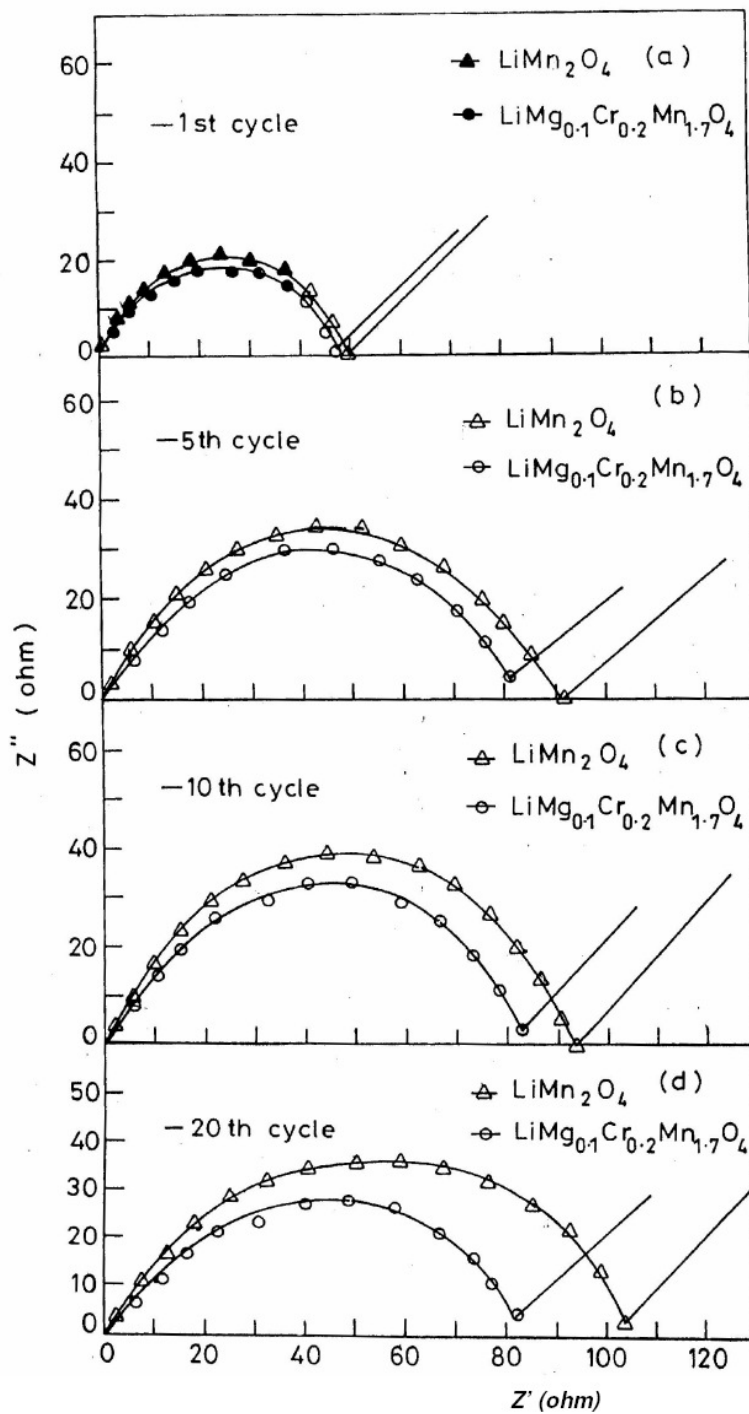**Figure 7.** Nyquist plots of $LiMn_2O_4$ and $LiMg_{0.1}Cr_{0.2}Mn_{1.7}O_4$ (1st, 5th, 10th and 20th cycles).

References

1. Y. Xia, M. Yoshio, *J. Electrochem. Soc*. 144 (1977) 2593.

2. G. Pistoia, A. Antonini, R. Rosati, D. Zane, *Electrochim. Acta* 41 (1996) 2863.

3. D.H. Jiang, J.Y. Shin, S.M. Oh, *J. Electrochem. Soc*. 143 (1996) 2204.

4. R.J. Gummow, A. de Kock, M.M. Thackeray, *Solid State Ionics* 69 (1994) 59.

5. A. Yamada, *J. Solid State Chem*. 122 (1996) 160.

6. G. Pistoia, G. Wang, C. Wang, *Solid State Ionics* 58 (1992) 285.

7. T. Ogihara, T. Yanagawa, M. Ogata, K. Yoshida, Y. Mizuno, S. Yonezawa, T. Takashima, N. Nagata, K. Gawa, *J. Ceram. Soc. Jpn*. 101 (1993) 1159.

8. G.L. Messing, S.C. Zhang, G.V. Javanthi, *J. Am. Ceram. Soc*. 76 (1993) 2707.

9. M.M. Thacheray, *J. Electrochem. Soc*. 142 (1995) 2558.

10. L. Guohua, H. Ikuta, T. Uchida, M. Wakihara, *J. Electrochem. Soc*. 143 (1997) 178.

11. A.D. Robertson, S.H. Lu, W.F. Averil, W.F. Howard, *J. Electrochem. Soc*. 144 (1977) 3500.

12. A.D. Robertson, S.H. Lu, W.F. Howard, *J. Electrochem. Soc*. 144 (1977) 3505.

13. A. Arora, G. Zheng, B.N. Popov, R.E. White, Electrochemical Society Meeting, Montreal, Canada, Vol. 97-1, Abstract Nº 90, p. 104 (1997).

14. G.B. Appetecchi, B. Scrosati, *Denki Kagaku* 66 (1998) 1299.

15. T. Ogihara, N. Ogata, S. Yonezawa, M. Takashima, N. Mizutani, *Denki Kagaku* 66 (1988) 1202.

16. T. Ogihara, N. Ogata, N. Mizutani, Electroceramics in Japan. 1. Trans. Tech. Publ. Ltd, Switzerland. 1988. p. 303.

17. T. Ogihara, A. Aikiyo, N. Ogata, N. Mizutani, *Adv. Powder Technol.* 10 (1999) 167.

18. A. Sigala, D. Guyomard, A. Verbaere, Y. Piffard, M. Tournoux, *Solid State Ionics* 81 (1995) 167.

19. Ullmann's Encyclopaedia of Industrial Chemistry, Vol. A16, 5th Ed., VCH Verlag. mbH, Weinheim, 1990, p. 31.

20. Ullmann's Encyclopaedia of Industrial Chemistry, Vol. A15, 5th Ed., VCH Verlag. mbH, Weinheim, 1990, p. 596.

21. D.R. Lide (Ed.), Handbook of Chemistry and Physics, 74th Ed., The Chemical Rubber Company, Ohio, 1993-1994, p. 203.

22. A. Lundbald, B. Bergman, *Solid State Ionics* 96 (1997) 173.

23. W.U. Malik, D.R. Gupta, I. Masood, R.S. Gupta, *J. Mater. Sci. Lett*. 4 (1985) 532.

24. A. Reisman, I.Ya. Lyubimtsera, L.A. Taiovkina, Yu. Krasnov, *Russ. J. Inorg. Chem*. 16 (1971) 130.

25. M.V. Smirnov, I.Ya. Lyubimtsera, L.A. Taiovkina, Yu. Krasnov, *Russ. J. Inorg. Chem*. 16 (1971) 130.

26. W. Baochem, X. Yongyao, F. Li, Z. Dongjiang, *J. Power Sources* 43-44 (1993) 108.

27. M.M. Thackeray, W.I.F. David, P.G. Bruce, J.B. Goodenough, *Mater. Res. Bull*. 19 (1983) 461.

28. M.M. Thackeray, P.J. Johnson, L.A. de Piccitto, P.G. Bruce, J.B. Goodenough, *Mater. Res. Bull*. 19 (1984) 179.

29. W.I.F. David, M.M. Thackeray, P.G. Bruce, J.B. Goodenough, *Mater. Res. Bull*. 19 (1984) 99.

30. M.M. Thackeray, A. de Koch, M.H. Rossouw, D.C. Liles, D. Hoge, R. Bittihn, *J. Electrochem. Soc*. 139 (1992) 363.

31. K.M. Kolbow, J.R. Dahn, R.R. Haering, *J. Power Sources* 26 (1989) 397.

32. W. Borchardt-ott. Crystallography. Springer, New York, 1993, p. 105.

33. A.F. Wells, Structural Inorganic Chemistry, 3rd Ed, Claredon press, Oxford, 1982, p.489.

34. T.J. Richardson, S.J. Wen, K.A. Striebel, P.N. Ross, E.J. Cairns, *Mater. Res. Bull*. 32 (1997) 609.

35. M. Tabuchi, K. Ado, M. Kobavashi, H. Sakebae, H. Hageyama, E. Masquelier, M. Yoneura, A. Hirano, R. Kanno, *J. Mater. Chem.* 9 (1999) 199.